Rare decays at LHCb

I. Belyaev

LAPP-EXP 2005-03
February 2005

Rare decays at LHCb

I. Belyaev

LAPP-IN2P3-CNRS
BP. 110, F-74941 Annecy-le-Vieux Cedex
and
Institute for Theoretical and Experimental Physics
Moscow, Russia

in Proceedings of the Conference "Physics at LHC"
Vienna, Austria, 13-14 July 2004

Rare decays at LHCb[1]

I. Belyaev[2]

Laboratoire d'Annecy-Le-Vieux de Physique des Particules,
Annecy-Le-Vieux, France
and
Institute for Theoretical and Experimental Physics,
Moscow, Russia

Abstract

Rare loop-induced decays are sensitive to New Physics in many Standard Model extensions. In this paper we discuss the reconstruction of the radiative penguin decays $B_d^0 \to K^{*0}\gamma$, $B_s^0 \to \phi\gamma$, $B_d^0 \to \omega\gamma$, the electroweak penguin decay $B_d^0 \to K^{*0}\mu^+\mu^-$, the gluonic penguin decays $B_d^0 \to \phi K_S^0$, $B_s^0 \to \phi\phi$ and the decay $B_s^0 \to \mu^+\mu^-$ at LHCb. The selection criteria, evaluated efficiencies, expected annual yields and $\mathcal{B}/\mathcal{S}$ estimates are presented.

[1]Proceedings of the conference "Physics at LHC", 13-14 July 2004, Vienna, Austria

[2]ibelyaev@lapp.in2p3.fr

1 Introduction

Studies of the rare radiative penguin decays $B^0_d \to K^{*0}\gamma$, $B^0_s \to \phi\gamma$, $B^0_d \to \omega\gamma$, the electroweak penguin decay $B^0_d \to K^{*0}\mu^+\mu^-$, the gluonic penguin decays $B^0_d \to \phi K^0_S$, $B^0_s \to \phi\phi$ and the decay $B^0_s \to \mu^+\mu^-$ allow to extract valuable information about penguin and box loop-diagrams (see Figure 1).

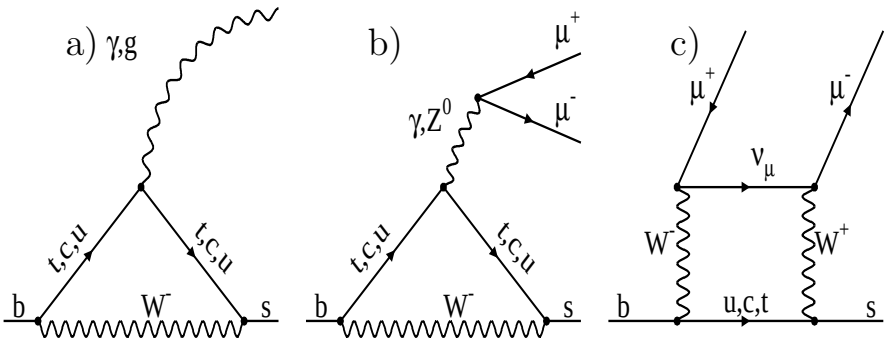

Figure 1: Loop diagrams which make the major contributions to $B^0_d \to K^{*0}\gamma$, $B^0_s \to \phi\gamma$, $B^0_d \to \omega\gamma$ (diagram **a** with a virtual photon), $B^0_d \to \phi K^0_S$, $B^0_s \to \phi\phi$ (diagram **a** with a virtual gluon), $B^0_d \to K^{*0}\mu^+\mu^-$ (diagrams **b** and **c**), $B^0_s \to \mu^+\mu^-$ (diagram **c**) decays.

Such diagrams are suppressed in the Standard Model (SM) due to GIM cancellation of different quark contributions. This cancellation is perfect in the limit of equal quark masses due to unitarity of the CKM-matrix. New particles arising in SM extensions in general do not preserve this cancellation and manifest themselves in particular in enhancements of loop amplitudes. For example the $B^0_s \to \mu^+\mu^-$ rate, predicted to be 3.5×10^{-9} in the SM [1], is enhanced by a factor $\tan^6\beta$ in SUSY models [2].

The complex couplings of new particles may result in the appearance of non-trivial $\mathcal{CP}$-violating phases, disturbing the $\mathcal{CP}$-asymmetries predicted by the SM. For example for the decay $B^0_d \to K^{*0}\gamma$ due to one-diagram dominance (the strong phase appears only at order α_S and $1/m_b$) the direct $\mathcal{CP}$-asymmetry is reliably predicted in the SM to be ≤ 1 % [3], but for some SUSY scenarios it could be as large as 10-40 % [3, 4].

Due to the $V-A$ structure of the weak current the photon polarization in $b \to s\,(d)\,\gamma$ transitions is almost 100%f. In the SM this causes the mixing-induced CP-asymmetries to vanish [5], while in extensions of the SM these asymmetries could be as large as 50 % [6]. This effect can be used as a probe for the spin structure of new particles.

The forward-backward asymmetry $\mathcal{A}_{\mathcal{FB}}(q^2)$ for the decay $B^0_d \to K^{*0}\mu^+\mu^-$, is defined through the angle $\theta_{\mathcal{FB}}$ between the μ^+ and K^{*0} momenta in the di-muon rest frame[3]. The shape of the asymmetry $\mathcal{A}_{\mathcal{FB}}(q^2)$ and especially the position of the zero crossing in the SM are almost unaffected by hadronic form factor uncertainties, thus providing a good basis for searching for deviations [7].

The discrepancy between the recent measurement of mixing-induced $\mathcal{CP}$ asymmetry in $B^0_d \to \phi K^0_S$ by the Belle collaboration [8] and the world average for the parameter $\sin 2\beta$ measured in charmonium modes [9] points to the necessity for careful and intensive studies of gluonic penguin dominated decays.

The test of QCD models in radiative penguin decays still plays an important role [10]. The ratio $|V_{td}|\ /|V_{ts}|$ could be extracted from $\Gamma(B^0_d \to \omega\gamma)/\Gamma(B^0_d \to K^{*0}\gamma)$ with moderate theoretical uncertainty.

2 Reconstruction of B-decays at LHCb

LHCb is a forward spectrometer at LHC. The detector has been described elsewhere [11–13]. The reconstruction of rare B-decays at LHCb is a challenge due to the small rates and large backgrounds from various sources. The most critical background is combinatorial background from $pp \to b\bar{b}X$ events, containing primary and secondary vertices and characterized by high charged and neutral multiplicities. We studied the forward $pp \to b\bar{b}X$ production as the dominating background, where at least one b-hadron is emitted forward within 400 mrad of the beam axis.

The studies have been performed using fully simulated events [13]. A detailed description of the charged particle identification in LHCb, based on a combined analysis of information from Čerenkov Detectors, Muon and Calorimeter Systems can be found elsewhere [13–17]. Photon candidates have been defined as clusters in the electromagnetic calorimeter not associated with any charged track [13, 16–18]. The reconstruction of π^0 and K^0_S is described in [13, 18, 19].

The background suppression exploits the generic properties of beauty production at pp-collisions. The large mass of beauty hadrons results in hard transverse momentum spectra of secondary particles. The large lifetime, $\langle\beta\gamma c\tau\rangle \sim 5$ mm, results in a good isolation of the B decay vertex and the inconsistency of B-decay products with the reconstructed pp-collision vertex.

For events with several reconstructed primary vertices the primary vertex

[3] q^2 is the di-muon invariant mass squared

with the minimum $B_d^0\,(B_s^0)$-candidate impact parameter has been chosen as the $B_d^0\,(B_s^0)$ production vertex [13].

2.1 Radiative penguin decays $B_d^0 \to K^{*0}\gamma$, $B_s^0 \to \phi\gamma$ and $B_d^0 \to \omega\gamma$

K^{*0} and ϕ candidates have been reconstructed [13, 21, 22] in the $K^+\pi^-$ and K^+K^- modes respectively[4].

Identified charged tracks have to be inconsistent with any reconstructed primary vertex. This requirement is especially effective to suppress combinatoric background for events with multiple pp-interactions [21]. A vertex fit has been applied to two tracks forming $K^{*0}\,(\phi)$ candidates. The mass window of $K^+\pi^-\,(K^+K^-)$ combinations has been chosen to be $\pm 60(10)$ MeV/c^2 around the nominal $K^{*0}\,(\phi)$ mass[5].

Selected $K^{*0}\,(\phi)$ candidates have been combined with photon candidates. The requirement on the transverse energy of the photon candidate to be greater than 2.8 GeV efficiently removes low energy γ and π^0. The transverse energy of the photon candidate with respect to the $B_d^0\,(B_s^0)$ candidate flight direction has to be within the interval $2.2\,(2.0) - 2.7$ GeV.

After these requirements the contribution from real K^{*0} in $pp \to b\bar{b}X$ inclusive events becomes smaller than combinatorial $K^+\pi^-$ background, while in the case of $B_s^0 \to \phi\gamma$ the remaining background comes mainly from real ϕ [21, 22]. The better background conditions for the low-mass di-kaon system permit to apply less tight cuts on the photon transverse energy for the reconstruction of $B_s \to \phi\gamma$ candidates.

The $K^{*0}\,(\phi)$ decay vertex has been considered as the $B_d^0\,(B_s^0)$-decay vertex. The angle θ_B between the momentum vector of the reconstructed $B_d^0\,(B_s^0)$ candidate and the flight path vector from the $B_d^0\,(B_s^0)$ production to the $B_d^0\,(B_s^0)$ decay vertices is required to be smaller than 6(15) mrad. This requirement is one of the most powerful cuts against combinatorial background as demonstrated in Figure 2. The smaller opening angle between the two kaons results in a larger uncertainty in the position of the secondary vertex, and therefore degraded resolution in θ_B.

Background from the decays $B_d^0 \to K^{*0}\pi^0$ and $B_s^0 \to \phi\pi^0$ with an energetic π^0 reconstructed as a single photon has been suppressed by requiring that $|\cos\vartheta| < 0.7$, where ϑ is the helicity angle between the B and the K^+ in the $K^{*0}\,(\phi)$ rest frame.

The invariant mass distributions of the selected and triggered $B_d^0 \to K^{*0}\gamma$

[4]The charge conjugate mode is always implied unless explicitely stated otherwise

[5]The cut values given in parentheses have been applied to the $B_s^0 \to \phi\gamma$ selection

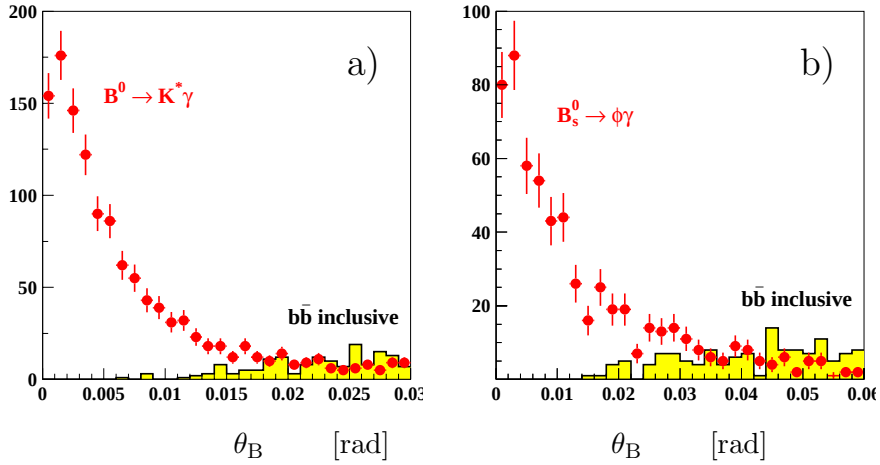

Figure 2: Distributions of the angle θ_B for signal events (points with error bars) and forward pp $\to$ b$\bar{\text{b}}$X events (filled histogram): a) $B_d^0 \to K^{*0}\gamma$, b) $B_s^0 \to \phi\gamma$.

and $B_s^0 \to \phi\gamma$ candidates are shown in Figures 3a and 3b. In both cases the mass resolution has been found to be ~ 65 MeV/c^2.

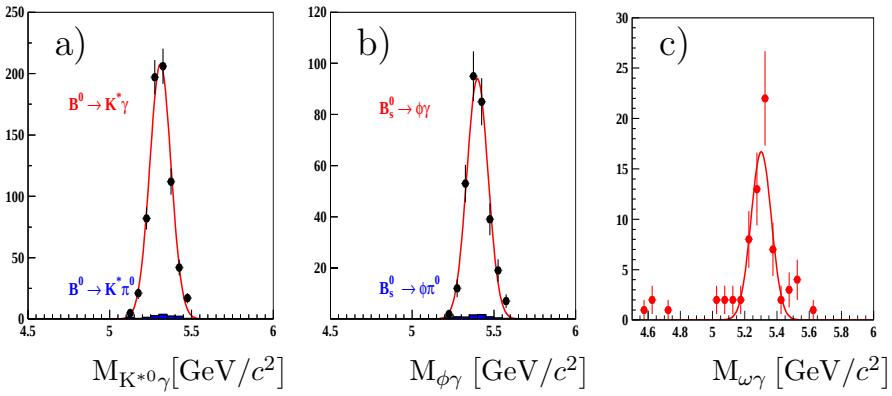

Figure 3: Invariant mass distributions for signal events after trigger and selection cuts: a) $B_d^0 \to K^{*0}\gamma$, b) $B_s^0 \to \phi\gamma$, c) $B_d^0 \to \omega\gamma$. The absolute normalization is arbitrary. The specific background from $B_d^0 \to K^{*0}\pi^0$ and $B_s^0 \to \phi\pi^0$ decays is shown in on a) and b) with proper normalization.

The selection of the decay $B_d^0 \to \omega\gamma$ followed by $\omega \to \pi^+\pi^-\pi^0$ follows a similar approach, but it is complicated by the π^0 reconstruction [18]. The invariant mass distribution for the selected and triggered $B_d^0 \to \omega\gamma$ candidates is shown in Figure 3c.

The selection efficiencies, which include acceptance and reconstruction

have been evaluated to be 0.41 %, 0.64 % and 0.03 % for $B_d^0 \to K^{*0}\gamma$,$B_s^0 \to \phi\gamma$ and $B_d^0 \to \omega\gamma$ channels respectively [21, 22].

2.2 Electroweak penguin decay $B_d^0 \to K^{*0}\mu^+\mu^-$

Di-muon candidates have been selected [23,24] from muons with a transverse momentum in excess of 900 MeV/c, originating from a common vertex. Di-muon candidates with an invariant mass in the mass intervals populated by $J/\psi \to \mu^+\mu^-$ and $\psi\,(2S) \to \mu^+\mu^-$ decays[6] have been excluded from the analysis.

$K^+\pi^-$ combinations with an invariant mass in the interval of ± 100 MeV/c^2 around the nominal K^{*0} mass and originating from common vertex have been considered as K^{*0} candidates. The transverse momentum of pions from K^{*0} candidates has been required to be larger than 200 MeV/c^2.

A vertex fit has been applied for pairs of selected di-muon and K^{*0} candidates. The significance of the B_d^0 impact parameter with respect to its production vertex has been required to be small, while a lower cut has been applied on the significance of the distance between the production vertex the B_d^0-decay vertex. Kaons and pions from the K^{*0} are required to be inconsistent with the B_d^0-production vertex. In addition a cut has been applied on the maximum multiplicity of tracks consistent with the B_d^0-decay vertex. This requirement improves the isolation of the B_d^0 decay vertex.

The invariant mass distribution for signal events after selection cuts is shown in Figure 4a. The B_d^0 mass resolution has been found to be 15 MeV/c^2. The distributions for the di-muon invariant mass and the angle $\theta_{\mathcal{FB}}$ are not distorted by acceptance or selection cuts, as illustrated in Figures 4b and 4c. The resolution on these observables has been estimated to be 9.7 MeV/c^2 and 4 mrad respectively.

The selection efficiency has been evaluated to be 0.96 %. The final state with a di-muon candidate has a trigger efficiency for selected events of 74 % [23].

2.3 Gluonic penguin decays $B_s^0 \to \phi\phi$ and $B_d^0 \to \phi K_S^0$

Kaons inconsistent with any reconstructed primary vertex in the event have been used for the recontruction of ϕ candidates [25–27]. A vertex fit has been applied to K^+K^- pairs and a mass window of $\pm 12(17)$ MeV/c^2 around the nominal ϕ mass has been chosen [7].

[6] The excluded intervals have been defined as $2.9 - 3.2$ and $3.65 - 3.75$ GeV/c^2

[7] The cut values given in parentheses has been applied to the $B_d^0 \to \phi K_S^0$ selection

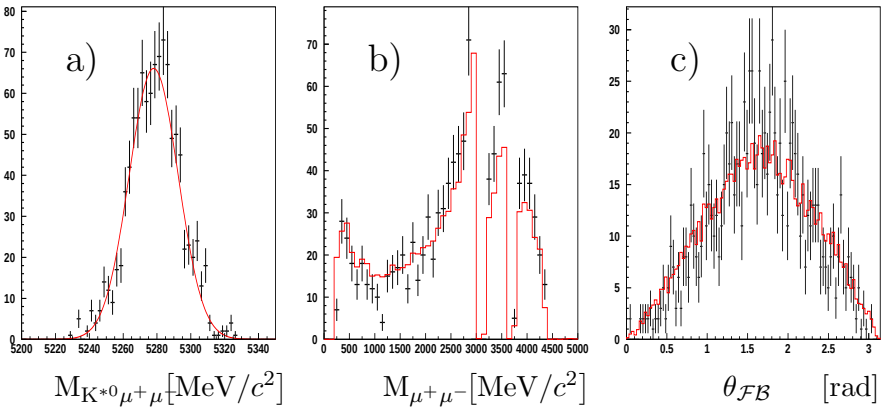

Figure 4: a) The $K^{*0}\mu^+\mu^-$ invariant mass distribution for $B^0_d \to K^{*0}\mu^+\mu^-$ events. The distributions of $\mu^+\mu^-$ invariant mass (b) and angle $\theta_{\mathcal{FB}}$ (c) for $B^0_d \to K^{*0}\mu^+\mu^-$ events (points with error bars), superimposed with the scaled distributions at generator level (solid histogram).

K^0_S candidates have been reconstructed as a $\pi^+\pi^-$ pair originating from a common secondary vertex. Three different categories of charged tracks have been used for the K^0_S reconstruction: *long* (tracks with hits both in the vertex detector before the magnet and the main tracker system after the magnet), *downstream* (tracks with no hits in the vertex detector) and *upstream* (tracks with no hits in the main tracker system) [13, 19]. The mass window has been defined to be ± 25 MeV/c^2 for pairs of two *downstream* tracks and ± 15 MeV/c^2 for all other combinations [19, 26, 27]. The transverse momentum of K^0_S candidates has been required to be greater than 1.1 GeV/c for K^0_S candidates from pairs of *downstream* tracks and greater then 500 MeV/c for all other combinations.

Pairs of selected ϕ from a common vertex have been considered as B^0_s candidates if the decay angle θ between the ϕ momentum in the rest frame of the $\phi\phi$ system and the direction of the Lorentz boost from the laboratory frame to the $\phi\phi$ rest frame satisfies $|\cos\theta| < 0.75$. Pairs of selected ϕ and K^0_S have been considered as B^0_d candidates if they originate from a common vertex and the transverse momentum of the ϕ exceeds 1.35 GeV/c^2. A cut on the minimal impact parameter of the ϕK^0_S pair with respect to all primary vertices has been used to suppress further the background. The value of this cut has been choosen to be 250 μm, 200 μm and 100 μm for K^0_S candidates recontructed from *downstream-downstream*, *long-long* pairs and other combinations correspondingly. The opening angle between the momentum of the B^0_s (B^0_d) candidate and the flight path vector has been required to be smaller than 10(15) mrad. The cut can be tighter in the case of $B^0_s \to \phi\phi$ decay since

the 4-prong $\phi\phi$ vertex provides for a better vertex resolution.

The invariant mass distributions of the selected and triggered $B_s^0 \to \phi\phi$ and $B_d^0 \to \phi K_S^0$ candidates are shown in Figures 5a and 5b. The mass resolutions for B_s^0 and B_d^0 decays have been found to be 12 MeV/c^2 and 16 MeV/c^2, respectively.

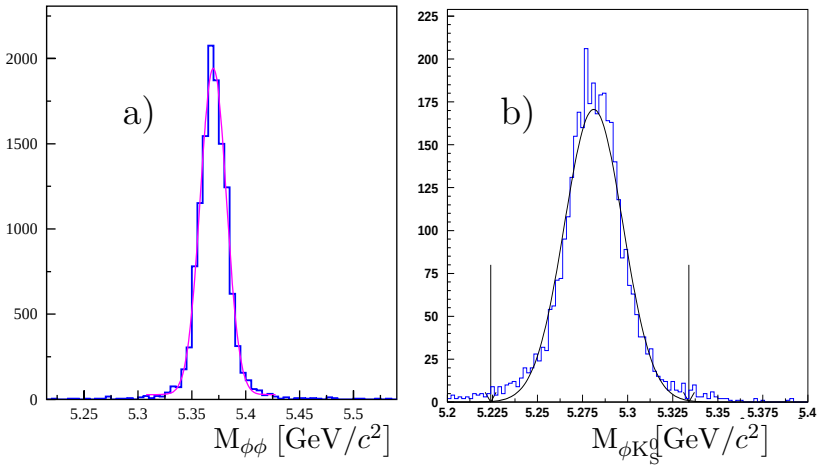

Figure 5: The invariant mass of B_s^0 (B_d^0) candidates after selection and trigger cuts: a) $B_s^0 \to \phi\phi$, b) $B_d^0 \to \phi K_S^0$

The selection efficiency has been evaluated to be 2.0 % and 1.1 % for $B_s^0 \to \phi\phi$ and $B_d^0 \to \phi K_S^0$ channels, respectively [25–27].

2.4 Decay $B_s^0 \to \mu^+\mu^-$

Since two-body B_s^0-decays are characterized by high transverse momenta of the decay products (see Figure 6a), only muons with a transverse momentum in excess of 1.5 GeV/c have been selected for the $B_s^0 \to \mu^+\mu^-$ reconstruction [28]. A vertex fit has been applied for di-muon combinations. The transverse momentum of muon pairs has been required to exceed 3.5 GeV/c^2. Di-muons with a small impact parameter with respect to the chosen primary vertex have been considered as B_s^0 candidates.

For selected B_s^0 candidates the separation between the reconstructed di-muon vertex and the primary vertex has been required to be large.

The invariant mass distribution for signal $B_s^0 \to \mu^+\mu^-$ events after selection and trigger cuts is shown in Figure 6b. The dimuon invariant mass resolution has been found to be 18 MeV/c^2.

The selection efficiency has been evaluated to be 3.1 %. The trigger efficiency for events that passed the selection criteria has been found to be 79 %.

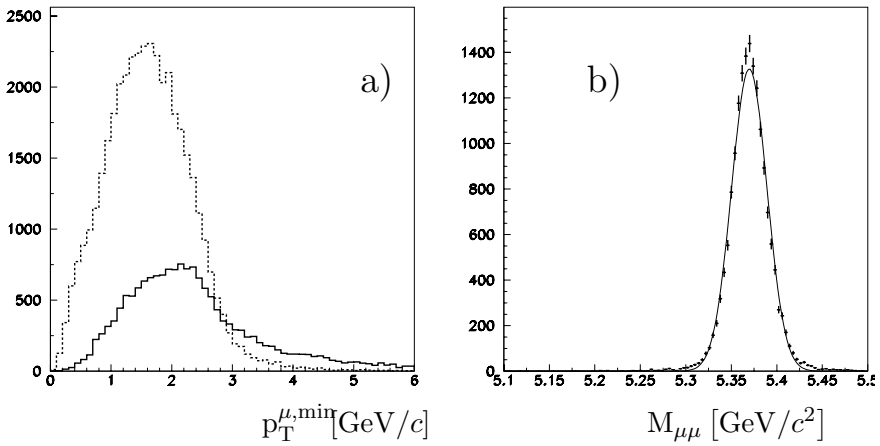

Figure 6: a) Distributions of the minimum transverse momentum of the particle from $\mu\mu$-pair for $B_s^0 \to \mu^+\mu^-$ and pp $\to$ (b $\to \mu$X) $\left(\bar{\text{b}} \to \mu\text{X}\right)$ X events (solid and dashed histograms correspondingly); b) The di-muon invariant mass distribution for $B_s^0 \to \mu^+\mu^-$ events after selection and trigger criteria.

2.5 Signal yields

The expected annual signal event yields (for 2 fb^{-1} accumulated luminosity) together with a summary of the estimated selection and trigger efficiencies are presented in Table 1.

Table 1: Selection (ε_{SEL}) and trigger (ε_{TRG}) efficiencies and the expected annual event yields for rare B-decays.

Channel	ε_{SEL} [%]	ε_{TRG} [%]	Yield
$B_d^0 \to K^{*0}\gamma$	0.41	38	$3.5 \cdot 10^4$
$B_s^0 \to \phi\gamma$	0.64	34	$9.3 \cdot 10^3$
$B_d^0 \to \omega\gamma$	0.03	37	40
$B_d^0 \to K^{*0}\mu^+\mu^-$	0.96	74	$4.4 \cdot 10^3$
$B_d^0 \to \phi K_S^0$	1.1	19	$0.8 \cdot 10^3$
$B_s^0 \to \phi\phi$	2.0	23	$1.2 \cdot 10^3$
$B_s^0 \to \mu^+\mu^-$	3.1	79	17

In the evaluation of trigger efficiencies, a 100 % efficiency for the High Level Triggers has been assumed. Other assumptions, parameters and branching ratios used for the evaluation of signal yields can be found elsewhere [13, 21–28].

2.6 Evaluation of background-to-signal ratio

As mentioned in Section 2, the forward $pp \to b\bar{b}X$ production is considered as the dominant background. The background from minimum bias events can be significant, but it has been assumed that this contribution is drastically suppressed at the trigger level, which exploits the hard transverse momentum spectra of b-decay products and large impact parameters of tracks from b-decays with respect to primary vertices [20].

To cope with the limited available Monte Carlo statistics, the B_d^0 (B_s^0) mass cut has been relaxed when analyzing these events. The background under the B_d^0 (B_s^0) mass peak has been estimated assuming a linear dependence on the reconstructed B_d^0 (B_s^0) mass (after removal of events with a true signal decay or similar decays which necessarily lead to a reconstructed mass outside the tight mass window). The definitions of tight and enlarged mass intervals used for the evaluation of background-to-signal ratios are listed in Table 2. In addition, in order to further increase the effective $pp \to b\bar{b}X$ statistics, all $\mathcal{B}/\mathcal{S}$ ratios have been estimated without applying the trigger criteria.

Table 2: Definition of tight (δM) and enlarged (ΔM) mass intervals and the estimated $\mathcal{B}_{b\bar{b}}/\mathcal{S}$ ratios (upper limits at 90 % confidence level) for forward $pp \to b\bar{b}X$ background

Channel	δM $[\mathrm{MeV}/c^2]$	ΔM $[\mathrm{GeV}/c^2]$	$\mathcal{B}_{b\bar{b}}/\mathcal{S}$
$B_d^0 \to K^{*0}\gamma$	± 200	$[4.6, 6.0]$	< 0.7
$B_s^0 \to \phi\gamma$	± 200	$[4.6, 6.0]$	< 2.4
$B_d^0 \to \omega\gamma$	± 200	$[4.6, 6.0]$	< 3.5
$B_d^0 \to K^{*0}\mu^+\mu^-$	± 50	± 1.0	< 2.0
$B_s^0 \to \phi\phi$	± 24	$[4.0, 7.0]$	< 0.2
$B_d^0 \to \phi K_S^0$	± 55	$[4.0, 6.6]$	< 1.1
$B_s^0 \to \mu^+\mu^-$	± 60	± 0.6	< 440

Except for the $B_d^0 \to K^{*0}\mu^+\mu^-$ channel, where two background events are selected, no background events from the available sample of 10^7 $pp \to b\bar{b}X$ events have passed the selection criteria in the enlarged mass interval. The 90 % confidence level upper limits set for the ratio of background from $pp \to b\bar{b}X$ events to signal are listed in Table 2.

The relative contribution of the correlated background from $B_d^0 \to K^{*0}\pi^0$ and $B_s^0 \to \phi\pi^0$ decays to the radiative penguin decays $B_d^0 \to K^{*0}\gamma$ and $B_s^0 \to \phi\gamma$ has been estimated to be small ($\mathcal{B}_{K^{*0}\pi^0}/\mathcal{S} < 2.2$ % for $B_d^0 \to K^{*0}\gamma$

and $\mathcal{B}_{\phi\pi^0}/\mathcal{S} < 4.0$ % for $\mathrm{B_s^0} \to \phi\gamma$) [21, 22].

The relative background contribution from inclusive ϕ production in b-decays to selected $\mathrm{B_d^0} \to \phi\mathrm{K_S^0}$ events has been estimated to be $B_{\mathrm{b}\to\phi}/S < 0.28$. A sample of 10^6 fully simulated $\mathrm{pp} \to (\mathrm{b} \to \phi\mathrm{X})\,\mathrm{X}$ events has been analysed [26, 27].

For the $\mathrm{B_d^0} \to \mathrm{K^{*0}}\mu^+\mu^-$ analysis, events with di-muons have been studied as potential background. Samples of 10^7 fully simulated $\mathrm{pp} \to (\mathrm{b} \to \mu\mathrm{X})\left(\bar{\mathrm{b}} \to \mu\mathrm{X}\right)\mathrm{X}$ and 2×10^5 $\mathrm{pp} \to (\mathrm{b} \to \mu^-\,(\mathrm{c} \to \mu^+\mathrm{X})\,\mathrm{X})\,\mathrm{X}$ events have been used. The contribution of the background with two primary muons from b-decays has been evaluated to be $\mathcal{B}_{\mu\mu}/\mathcal{S} = 0.5 \pm 0.2$. The contribution of the background with one primary and one cascade muon has been evaluated to be $\mathcal{B}_{\mu\mu'}/\mathcal{S} < 1.1$. Contributions from the exclusive decays $\mathrm{B_d^0} \to \mathrm{J/\psi K^{*0}}$, $\mathrm{B_d^0} \to \mathrm{J/\psi K_S^0}$ and $\mathrm{B_s^0} \to \mathrm{J/\psi}\phi$ have been found to be smaller than < 5 % each [23, 24].

The feed-down to selected $\mathrm{B_s^0} \to \mu^+\mu^-$ events from exclusive two-prong decays of b-hadrons with misidentified muons has beed evaluated to be an order of magnitude smaller than the signal yield in a ± 25 MeV/c^2 window around the nominal $\mathrm{B_s^0}$ mass [29]. The background contribution from $\mathrm{pp} \to (\mathrm{b} \to \mu\mathrm{X})\left(\bar{\mathrm{b}} \to \mu\mathrm{X}\right)\mathrm{X}$ events has been evaluated to be $\mathcal{B}_{\mu\mu}/\mathcal{S} < 5.7$ [28].

3 Conclusion

The LHCb experiment has promising physics potential for the study of numerous loop-induced rare decays such as the radiative penguin decays $\mathrm{B_d^0} \to \mathrm{K^{*0}}\gamma$, $\mathrm{B_s^0} \to \phi\gamma$ and $\mathrm{B_d^0} \to \omega\gamma$, the electroweak penguin decay $\mathrm{B_d^0} \to \mathrm{K^{*0}}\mu^+\mu^-$, the gluonic penguin decays $\mathrm{B_s^0} \to \phi\phi$ and $\mathrm{B_d^0} \to \phi\mathrm{K_S^0}$ and the rare box decay $\mathrm{B_s^0} \to \mu^+\mu^-$. The expected annual signal event yields and preliminary estimates on background-to-signal ratios have been presented.

The precision and reliability of background-to-signal estimations are expected to improve with a significant increase of Monte Carlo samples. Studies of high level trigger efficiencies, systematic uncertainties, and the sensitivity to new physics are in progress.

It is a great pleasure to thank the Drs. G. Pakhlova and S. Barsuk for extremely pleasant cooperation, Drs. S. Amato, O. Leroy, J.H. Lopes, F. Marinho, B. de Paula, B. Viaud, Y. Xie and Profs. E. Aslanides, R. Le Gac, A. Tsaregorodtsev for their contributions to this work, Drs. O. Deschamps, S. Easo, C. Jones, F. Machefert, P. Pakhlov, P. Koppenburg, F. Teubert, Profs. H. Dijkstra, R. Forty, A. Golutvin, T. Nakada, B. Pietrzyk, T. Ruf, S. Semenov, O. Schneider and O. Steinkamp for useful discussions.

References

[1] A. Ali, hep/ph 9702312 (1997)

[2] G. Buchalla and A.J. Buras, Nucl.Phys. **B398** 285 (1993)
G. Buchalla and A.J. Buras, Nucl.Phys. **B400** 225 (1993)
G. Buchalla and A.J. Buras, Nucl.Phys. CERN-TH-1998-369

[3] T. Hurth and T. Mannel, CERN-TH-2001-242

[4] M. Neubert, CLNS-03-1814

[5] M. Gronau, EFI-03-17

[6] D. Atwood, M. Gronau and A. Soni, Phys.Rev.Lett. **79** 185 (1997)
A. Masiero, TUM-HEP-303-97

[7] A. Ali, hep-ph/0210183 (2002)

[8] K. Abe *et.al.*, Phys.Rev.Lett. **91** 261602 (2003)

[9] S. Eidelman *at al.*, Phys.Lett. **B592**, 1 (2004)

[10] M. Neubert, hep-ph/0110301 (2001).

[11] H. Dijkstra *et al.*, LHCb-95-001

[12] S. Amato *et al.*, CERN-LHCC-98-004

[13] R. Antunes Nobrega *et al.*, CERN-LHCC-2003-030

[14] S. Amato *et al.*, CERN-LHCC-2000-037

[15] P.R. Barbosa Marinho *et al.*, CERN-LHCC-2001-010
P.R. Barbosa Marinho *et al.*, CERN-LHCC-2003-003

[16] S. Amato *et al.*, CERN-LHCC-2000-036

[17] H. Terrier and I. Belyaev, LHCb-2003-092

[18] O. Deschamps *et al.*, LHCb-2003-091

[19] Y. Xie, LHCb-2003-088

[20] R. Antunes Nobrega *et al.*, CERN-LHCC-2003-031

[21] G. Pakhlova and I. Belyaev, LHCb-2003-090

[22] G. Pakhlova, Czech. J. Phys. **54** (2004) Suppl. A

[23] J.H. Lopes, LHCb-2003-104

[24] J.H. Lopes, Czech. J. Phys. **54** (2004) Suppl. A

[25] S. Barsuk and I. Belyaev, LHCb-2003-094

[26] E. Aslanides *et al.*, LHCb-2004-001

[27] B. Viaud, Ph.D. Theses, CPPM-T-2003-06

[28] B. de Paula, F. Marinho and S. Amato, LHCb-2003-16

[29] E. Polycarpo, LHCB-2002-027
E. Polycarpo, Ph.D. Theses, CERN-THESIS-2002-023